

Microstructure and mechanical characterization of ZrC–Mo cermets produced by hot isostatic pressing

Sean E. Landwehr^a, Gregory E. Hilmas^{a,*}, William G. Fahrenholtz^a,
Inna G. Talmy^b, Stephen G. DiPietro^c

^a Materials Science and Engineering Department, Missouri University of Science and Technology, Rolla, MO 65409, USA

^b Ceramic Science Group, Naval Surface Warfare Center Carderock Division, West Bethesda, MD 20817, USA

^c Exothermics Inc., Amherst, NH 03031, USA

ARTICLE INFO

Article history:

Received 7 December 2007

Received in revised form 6 June 2008

Accepted 15 July 2008

Keywords:

Hot isostatic pressing

Zirconium carbide

Molybdenum

Cermet

Mechanical properties

ABSTRACT

Microstructure analysis and mechanical characterization were performed on ZrC–Mo composites with 20, 30, and 40 vol% Mo produced by hot isostatic pressing. The composites reached >98% relative density after processing at 1800 °C and 200 MPa for 1 h. The ZrC grain size was ~1–2 μm after densification. The Mo appeared to form clusters that increased in size from 15 to 54 μm with increasing Mo content. Analysis of mechanical property data indicated that the Mo clusters acted as the critical flaws during fracture. Hardness decreased from ~17 to ~8 GPa with increasing Mo content, and was related to the effective hardness of each of the constituent materials. The elastic moduli also decreased with Mo additions from 392 GPa (corrected for porosity) to ~380 GPa. Flexure strength and fracture toughness increased with increasing Mo content from 320 to 480 MPa and 1.0 to 6.6 MPa√m, respectively. The elastic moduli, flexure strength, and fracture toughness were all found to follow a volumetric rule of mixtures.

© 2008 Elsevier B.V. All rights reserved.

1. Introduction

To improve the performance in rocket propulsion systems, rocket fuel combustion temperatures are increasing while rocket motors are being made smaller. With this dichotomy, rocket propulsion materials must have increased ablation and erosion resistance to realize an improvement in performance. Refractory carbides are desirable in these applications due to melting temperature in excess of 3000 °C. Zirconium carbide, in particular, is of interest because of its combination of high-melting temperature (3445 °C) [1] and chemical resistance [2]. Unfortunately, ZrC, as with most ceramics, shows poor fracture toughness (~4.0 MPa√m) [3]. The fracture toughness and susceptibility to thermal shock damage have prevented the use of ZrC in propulsion applications to date. However, the fracture resistance of ZrC can be increased with the addition of refractory metals such as Nb, W, and Mo [4–10]. Most of these studies, and in particular the ZrC–Mo studies, have focused on arc-melted materials, with subsequent annealing to homogenize cast specimens [8–10]. This method was similar to the method used in the phase equilibria studies that have been performed in the system [11–13].

Previous studies performed by the authors of this paper demonstrated the chemical compatibility of ZrC and Mo, and showed that the materials could be densified by liquid phase sintering [14,15]. The first study was conducted on mixtures of a 1:1 molar ratio of ZrC:Mo both in carburizing and non-carburizing atmospheres. It was determined that processing in a carburizing environment was unsuitable due to the complete carburization of Mo to form Mo₂C. Heating in a He/H₂ atmosphere resulted in liquid formation between 2100 and 2200 °C, which was due to the eutectic melting interaction between Mo₂C formed during heating and unreacted Mo [14].

A further study was performed on pressureless densification of ZrC–Mo cermets. It was found that ZrC–Mo cermets could be liquid phase sintered by heating to 2150 °C in a He/H₂ atmosphere. The liquid phase formed due to the formation of Mo₂C, and its interaction with ZrC and Mo. The study also explored the ability to sinter the materials in the solid state. It was found that small specimens could be sintered to near full density at 2200 °C without a liquid phase, which resulted in a significantly different microstructure than the liquid phase sintered materials. Unfortunately, it was difficult to produce specimens for mechanical properties testing due to uneven distribution of pores in large specimens [15].

Pressure assisted sintering is a method to improve densification in the solid state. Conventional hot pressing with graphite-based systems was ruled out in the first compatibility study because of

* Corresponding author. Tel.: +1 573 341 6102; fax: +1 573 341 6934.
E-mail address: ghilmas@mst.edu (G.E. Hilmas).

a reaction between Mo and graphite to form Mo_2C [14]. Hot isostatic pressing (HIP), on the other hand, offers the ability to place the powders in a container that protects them from the graphite heating element and other carbon sources. HIP can also allow for lower sintering temperatures by promoting densification in preference to grain coarsening, resulting in a finer grain size in the final microstructure [16,17]. This presumed reduction in grain size would be expected to increase strength as well as improve hardness. In the current study, HIP was employed to densify ZrC with (nominally) 20, 30, and 40 vol% Mo. These composites were then characterized by measuring flexure strength, hardness, elastic modulus, and fracture toughness. The properties were then related to the microstructure of the materials.

2. Experimental procedure

2.1. Powder processing and HIP

Zirconium carbide powder ($<5\ \mu\text{m}$, Alfa Aesar 35808, Ward Hill, MA) was mixed with 20, 30, and 40 vol% Mo powder (average particle size $3\text{--}7\ \mu\text{m}$, Alfa Aesar 10030, Ward Hill, MA) and ball milled for 24 h. The powders were dried at 180°C under flowing N_2 . The dried powders were then dry ball milled to ensure homogeneity. After milling, the mixed powders were heated progressively in vacuum to 1000°C (over the course of $\sim 12\ \text{h}$) to remove any volatile species. Residual gas analysis was used to determine when all volatile species were removed. The powders were then vacuum-sealed in Ta cans for the HIP process. The specimens were pressed in the HIP (QIH-20, Kent, WA) with a pressure of 200 MPa for 1 h at 1800°C . Specimens were removed from the Ta cans by grinding.

2.2. Material characterization

The Archimedes' technique was used to measure the bulk density of the specimens after HIP. Water was used as the immersion medium. X-ray diffraction analysis (Scintag Inc., $\theta\text{--}\theta$ type XDS200 X-ray diffractometer, Cupertino, CA) was performed on ground and sieved specimens using a packed powder mount. Analysis used $\text{Cu K}\alpha$ radiation that had the $\text{K}\beta$ radiation removed by passing through a Ni filter. The accelerating voltage was 45 kV with a filament current of 40 mA. The scans used a step size of 0.03° and a count time of 0.5 s at each step. Lattice parameters of the ZrC phase were calculated by Rietveld refinement performed using Riqas software (Materials Data Inc., Livermore, CA). The calculated lattice parameters were compared to the literature values [11] to quantitatively determine the amount of Mo in solid solution with ZrC. Scanning electron microscopy (SEM; Hitachi S570, Tokyo, Japan) was used to examine polished cross-sections to characterize the microstructures.

Elastic properties were measured by impulse excitation using the method outlined in ASTM C1259. The specimens used for measurement were $5\ \text{mm} \times 13\ \text{mm} \times 80\ \text{mm}$. The fundamental frequency was measured (Grindosonic MK 4-I, J.W. Lemmens, St. Louis, MO) and used to calculate Young's modulus. The torsional frequency was measured and used to calculate the shear modulus. Poisson's ratio was calculated from the values obtained for Young's and shear moduli (assuming an isotropic material). This process was repeated for 10 specimens with each composition and the average is reported.

Hardness measurements were conducted according to ASTM C 1327-03. As per the standard, the indents were made by a Vickers diamond (Duramin 5, Struers, Ballerup, Denmark) at a load of 1 kg. The measured hardness value for each composition was taken as the average of 10 indents (as specified for multiple phase materials).

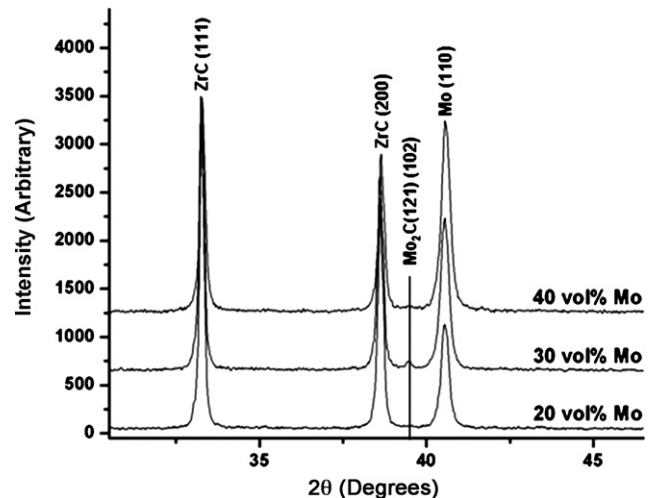


Fig. 1. XRD spectra for ZrC with 20, 30 and 40 vol% Mo after HIP at 1800°C and 200 MPa showing the presence of Mo_2C in the 30 vol% Mo specimen.

Flexural strength was determined using four-point bending (Instron 5881 Norwood, MA) in accordance with ASTM C1161-02. The test specimens used were type "B" bars ($3\ \text{mm} \times 4\ \text{mm} \times 45\ \text{mm}$) and were tested in a fully articulated fixture having an outer span of 40 mm with loading at the quarter points.

Fracture toughness was tested using a method modified from that outlined in ASTM C1421-01 for the surface crack in flexure test. The modified method did not include grinding the surface after indentation because of corrosion effects to the Mo in the material and using a Vickers' indenter instead of a Knoop indenter for flaw symmetry with respect to loading. The lack of grinding was compensated by using a large load (50 kg) on the indenter, which would drive the surface crack deeper and would mitigate any surface effects of the indent. The specimens were $3\ \text{mm} \times 4\ \text{mm} \times 25\ \text{mm}$ with the indentation placed on a 3 mm wide surface. The surface cracks initiated by the indent were measured with optical microscopy (HiRox KH-3000, River Edge, NJ), as this method appeared to give the greatest contrast on the fracture surface for accurate measurement of the surface crack.

3. Results and discussion

3.1. XRD

X-ray diffraction analysis was performed on each of the ZrC–Mo compositions. It was determined that the 20 and 40 vol% Mo contained only ZrC and Mo. The nominally 30 vol% Mo composition, however, contained trace amounts of Mo_2C (Fig. 1). Following the line of reasoning presented in previous studies [11], the absence of Mo_2C at the processing temperature of 1800°C was due to carbon deficiency in the system. The carbon deficiency was due to the reaction of O with C from the ZrC, similar to the ZrC–Mo cermets in a previous study [15] that were sintered in a neutral atmosphere (i.e., no reducing component in the process atmosphere). In this case, the reaction most likely took place during the heating to 1000°C under vacuum, which was intended to remove any remaining organic species. According to the thermodynamic calculations, the carbothermal reduction of MoO_2 to Mo is favorable above $\sim 800^\circ\text{C}$. This does not explain, however, why only the 30 vol% Mo composition contained Mo_2C , which may not be possible to determine with complete certainty with the current understanding of phase equilibria in the Zr–Mo–C system. It is clear, however, that

Table 1
Lattice parameters of ZrC and the corresponding amount of Mo in solid solution (ss)

Composition	Lattice parameter (Å)	Mo in ss (mol%) ^a
Hot Pressed ZrC	4.680	0.0
ZrC 20 vol% Mo	4.657	5.9
ZrC 30 vol% Mo	4.655	6.5
ZrC 40 vol% Mo	4.649	8.2

^a Values are ± 1.1 mol%.

enough carbon was left in that specimen to form a small amount of Mo₂C. The quantification of the amount of Mo₂C will be addressed in the next section.

From XRD analysis, the ZrC peaks were found to have shifted to higher 2θ values as compared to the stoichiometric compound, indicating Mo dissolution in ZrC. The amount of solid solution increased with increasing Mo content and the maximum Mo content in the ZrC was 8.3 mol% for the 40 vol% Mo composition (Table 1). This Mo content is near the solubility limit of solid solution that has been presented in previous studies [11,12,14]. The extent of solid solution was used along with other constraints to determine the amounts of each phase present in the final composites, which is presented in the next section.

3.2. Density and microstructure

The microstructure of HIP 20, 30 and 40 vol% Mo compositions were characterized by examining polished cross-sections using SEM. From Fig. 2, the Mo was in well-dispersed clusters that increased in size with increasing Mo content. On average, the clusters were 15, 22, and 54 μm for 20, 30 and 40 vol% Mo, respectively. The Mo may or may not form an interconnected phase in these composites. Typically, if the ceramic phase is an electrical insulator, the electrical resistivity (or conductivity) can be measured as function of metal content. The connectivity of the metal phase can then be determined based on the composition at which the electrical resistivity drops several orders of magnitude [18,19]. This method does not work for the ZrC–Mo system because of the similar electrical resistivities of ZrC and Mo (~ 65 and $5 \mu\Omega \text{ cm}$, respectively) [20,21]. However, in previous studies of hot pressed AlN–Mo composites, the microstructures were similar to the materials produced in this study and it was found that in the electrical resistivity decreased by about 10 orders of magnitude between 20 and 22 vol% Mo. The electrical resistivity also decreased by about 2 orders of magnitude between 15 and 20 vol% Mo. These observations suggest that the Mo in the hot pressed specimens, even HIP specimens, should become interconnected between 15 and 22 vol% Mo [18,19], forming a two phase, interpenetrating type microstructure.

The ZrC grain size was difficult to determine because of an inability to etch specimens by thermal or chemical means. However, some individual ZrC grains were observed within the Mo clusters (arrows in Fig. 2) and were 1–2 μm in size on average. This is about the size of the starting ZrC powder (which is $< 5 \mu\text{m}$), which leads to the conclusion that ZrC grain growth was minimal during densification. Minimal grain growth is typical of HIP processing [17], and is in stark contrast to the grain coarsening observed in liquid phase sintered materials [14,15].

The decrease in ZrC grain size from 5 to 30 μm in liquid phase sintered specimens to 1–2 μm in HIP specimens was not the only change observed [15]. As previously mentioned, the Mo was present in the specimens as clusters in the HIP specimens. This is different from the Mo morphology as a continuous phase (along with Mo₂C) that completely wets and surrounds the larger ZrC grains, in the liquid phase sintered specimens [15]. The microstructure of the HIP materials was, however, similar to that of specimens sintered

in vacuum in which the Mo appeared to be discontinuous and no Mo₂C formation was observed [15]. The HIP specimens also had a finer ZrC grain size (1–2 μm) than the pressureless sintered materials (5–40 μm) as would be expected with the lower processing temperature (1800 °C versus 2200 °C) and the application of pressure during sintering [15–17]. The biggest difference between the processes was the ability to densify ZrC–Mo by HIP without the scale-up problems experienced in the previous study with vacuum sintering.

As shown in Fig. 2 is the microstructure of a hot pressed ZrC specimen. Unlike the composite materials, the material without Mo could be thermally etched. The etched microstructure revealed large grains (5–50 μm) with porosity that was entrapped within the grains. This is typical for ZrC sintered with no additives, which typically reaches only 96–98% of theoretical density because excessive grain growth, prior to complete densification, leads to entrapped porosity [22–24].

Density measurement results (Table 2) were consistent with the amount and type of porosity that was observed in the microstructures. All specimens showed negligible open porosity ($< 1.5\%$). The density of the hot pressed ZrC was consistent with the porosity observed within the grains. Using the theoretical density, it was determined that the hot pressed ZrC contained 1.7% porosity, which was slightly less than the 3.2% determined by image analysis. However, image analysis may over estimate the amount of porosity due to chipping around existing porosity and grain boundaries during polishing.

For all of the HIP ZrC–Mo specimens, porosity was almost indiscernible by image analysis (at least for practical statistical analysis). To calculate the fraction of porosity in the specimens, the amount of Mo in solid solution with ZrC had to be determined (Table 1). For the 20 and 40 vol% Mo specimens, the amount of Mo in solid solution with the ZrC was simply subtracted from the original amount of Mo in the system to determine the amount of each phase to use in the volume rule of mixtures calculation for theoretical density. The calculation used the XRD theoretical densities of each phase. From this analysis, porosity values of 0.2, and 1.3 vol% were determined for the 20 and 40 vol% Mo compositions, respectively.

Due to the presence of Mo₂C in the 30 vol% Mo, the previous comparison between porosity determined by image analysis values and those determined theoretically, was difficult to make. However, using a similar method to the previous study in this series [15] the amount of Mo₂C was determined. In the previous study, image analysis was employed to determine the amount of total porosity in the specimen. As mentioned above, the volume of porosity was so low in the HIP processed materials that it was not possible to calculate it in this manner. As such, it was assumed that the specimens had reached full density and porosity was not factored into the calculation. Knowing the amount of Mo in solid solution with ZrC, and the assumed theoretical density, the volume rule of mixtures and conservation of mass law were used to determine the amount of Mo₂C, which was 2.4 vol%. This was a smaller than the amount of Mo₂C found in the liquid phase sintered materials, and the Mo₂C was not discernible as a distinct separate phase in SEM analysis as it was in liquid phase sintered ZrC–Mo [15].

3.3. Hardness

Vickers hardness was found to decrease with increasing Mo content. The maximum hardness was measured for ZrC at 20 GPa while ZrC–40 vol% Mo had a hardness of approximately 8 GPa (Fig. 3). Two models are plotted in Fig. 3 along with the measured values. The first model was developed to calculate the hardness model of WC–Co and was proposed by Lee and Gurland [25]. The model is mathematically described in Eq. (1), where H_C is the hardness of the

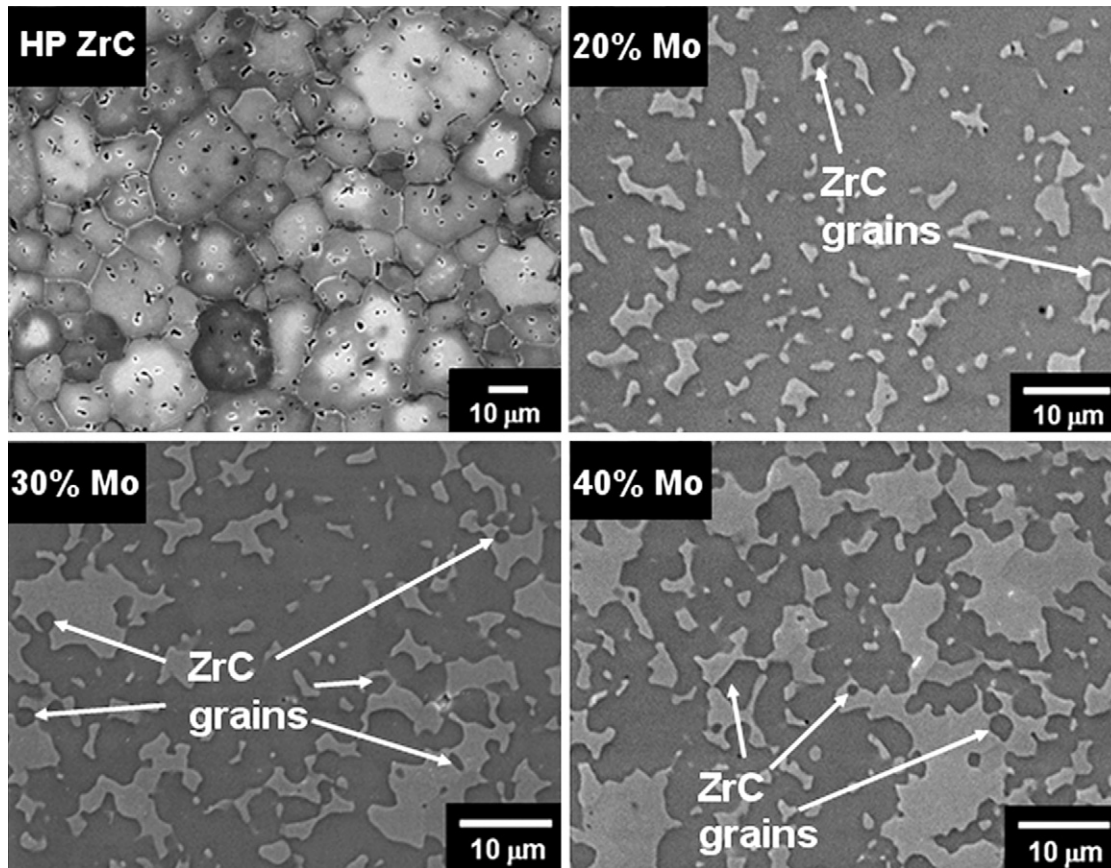


Fig. 2. SEM micrographs of ZrC hot pressed at 2200 °C and ZrC with 20, 30 and 40 vol% Mo after HIP at 1800 °C and 200 MPa. Mo is the lighter phase and ZrC is the darker phase. Examples of individual ZrC grains used for determining grain size are indicated by the arrows.

composite, H_{ZrC} is the effective hardness of ZrC, H_{Mo} is the effective hardness of the Mo phase, V_{ZrC} is the volume fraction of ZrC, and C is the contiguity of the ZrC phase. The effective hardness values are determined empirically and based on Hall–Petch behavior so that H_{ZrC} (Eq. (2)) increases with decreasing grain size, d , and H_{Mo} (Eq. (3)) increases with decreasing mean free path, λ (also a function of Mo volume fraction, f , and ZrC grain size). In Eq. (2) and (3), the curve fitting parameters a , b , m , and n are difficult to determine without extensive study so they were based on the hardness of hot pressed ZrC (average grain size of 10 μm) measured by Vickers indentation (20.1 GPa), and the hardness of a Mo alloy with additions of Ti and Zr (known as TZM with a hardness of 2.3 GPa) [26] since it was determined in previous studies that Zr (from ZrC) goes into solid solution with Mo [13,15]:

$$H_C = H_{ZrC}V_{ZrC}C + H_{Mo}(1 - V_{ZrC}C) \quad (1)$$

$$H_{ZrC} = a + \frac{b}{\sqrt{d}} \quad (2)$$

$$H_{Mo} = m + \frac{n}{\sqrt{\lambda}} \quad (3)$$

This model was developed to describe the hardness of WC–Co cermets, and is basically a volumetric rule of mixtures with an additional term, contiguity, that was defined by Gurland in an earlier study [27]. The contiguity term was added to describe the extent of connectivity of a particular phase (in this case the hard carbide phase in a WC–Co cermet), which has been shown to have a profound effect on many aspects of mechanical behavior [25,28]. The contiguity decreases approximately exponentially with increasing metal volume fraction [21]. Overall, the Lee and Gurland model describes the trend well, but appears to breakdown at Mo contents at 40 vol% Mo and above as shown by the deviation of the solid line from the measured hardness in Fig. 3.

The other model presented is that of Enqvist et al. [29]. This model was similar to the Lee and Gurland model, but rather than using a modified rule of mixtures, the model considered the hardening effect of the metal phase. Mathematically, this model is described by Eq. (4). In these equations, H_C is the composite hard-

Table 2
Post-processing composition and density measurements

Composition	(Zr,Mo)C (vol%)	Mo ss (vol%)	(Mo,Zr) ₂ C (vol%)	Calculated density (g/cm ³)	Measured density (g/cm ³)	Relative density (%)
Hot pressed ZrC	100.0	0.0	0.0	6.74	6.62	98.3
ZrC 20 vol% Mo	82.4	17.6	0.0	7.35	7.34	99.8
ZrC 30 vol% Mo	74.1 ^a	23.5 ^a	2.4 ^a	7.61 ^b	7.61 ^b	100.0
ZrC 40 vol% Mo	61.9	38.1	0.0	8.07	7.96	98.7

^a Values are $\pm 1.5\%$, all others are $\pm 1.1\%$.

^b 100% theoretical density was assumed to calculate amount of Mo₂C.

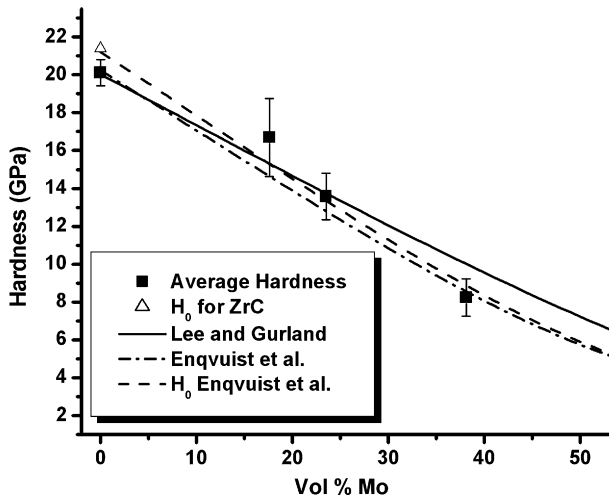


Fig. 3. Average measured hardness as a function of Mo content with two hardness models fit to the data including a model that compensates for the porosity in the hot pressed ZrC.

ness; H_{ZrC} and H_{Mo} are the effective hardness values for ZrC and Mo, respectively; λ is the mean free path of the metal; k is a curve fitting parameter. The empirically derived, effective hardness of the ZrC phase is given in Eq. (5), and is different from Eq. (2) by the addition of the curve fitting parameter c to give the second term a defined value if the grain size, d , goes to 0. Since the overall function is based on the hardening effect of the metal phase, the effective hardness of Mo in this equation is simply an empirically derived base value. The determination of H_{ZrC} was the same as with the Lee and Gurland model. The baseline H_{Mo} value was taken to be that of the TZM alloy. To create a hardness function dependent on Mo volume fraction, the mean free path was simply replaced with the product of grain size ($3 \mu\text{m}$) and volume fraction. The curve fitting parameter, k , was determined through trial and error:

$$H_C = (H_{ZrC} - H_{Mo})e^{-k/\lambda} - H_{Mo} \quad (4)$$

$$H_{WC} = a + \frac{b}{\sqrt{c+d}} \quad (5)$$

The Enqvist et al. model appears to provide a more consistent fit with measured hardness values than the Lee and Gurland model overall, but slightly underestimated the hardness of the 20 and 30 vol% Mo composites. This, however, was due to the assumption that the ZrC hardness was the same as the baseline hot pressed ZrC. As was shown previously, the hot pressed ZrC contained closed porosity, which should have reduced its hardness exponentially from the true hardness value as outlined by Wu and Rice [30].

The hardness correction for porosity outlined by Wu and Rice takes the general form found in Eq. (6). In the equation, H is the measured hardness, H_0 is the hardness of the material with no porosity, P is the volume fraction of porosity, and b is a characteristic number for the porosity that is based on shape and distribution. In this case, a b factor of 3 was used for the dispersed spherical porosity observed in the microstructure (Fig. 2).

$$H = H_0 e^{-bP} \quad (6)$$

When the hardness of ZrC was corrected for porosity, H_0 had a value of 21.5 GPa, which was about 7% greater than the value measured in the present study (Fig. 3). Using this higher value for the hardness of dense ZrC, the Enqvist model more accurately predicted the hardnesses of the 20 and 30 vol% Mo compositions (also shown in Fig. 3). It still slightly underestimates the hardness of the 20 and 30 vol% Mo composites, but falls within the variability of the mea-

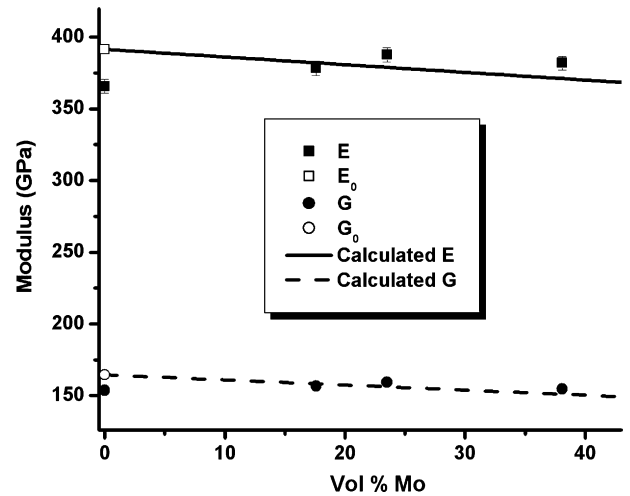


Fig. 4. Measured Young's and shear moduli of ZrC–Mo cermets as a function of Mo content along with the values calculated for full density (open circles) and values predicted from models.

sured values. Additional hardness testing of ZrC with grain sizes similar to the HIP composites, along with hardness measurements of a Mo material produced by HIP and having a similar composition, should yield an even more accurate prediction of hardness in the ZrC–Mo system.

3.4. Elastic moduli

The measured Young's and shear moduli for the ZrC–Mo composites are shown in Fig. 4. The elastic moduli were expected to decrease with increasing Mo content due to the lower Young's modulus for Mo (~ 330 GPa [31]) compared to ZrC (~ 392 GPa [32]). However, this was not the case as the hot pressed ZrC exhibited the lowest Young's (365 GPa) and shear (155 GPa) moduli. The Young's moduli were ~ 380 GPa and the shear moduli were ~ 160 GPa for all of the HIP materials. The trend in elastic moduli can be understood, if the effect of porosity in the hot pressed ZrC is considered. By applying the Spriggs relationship [33], which is similar to the hardness relationship described earlier, and is included as Eq. (7), it is possible to determine the intrinsic Young's modulus for ZrC (i.e., the value for no porosity). In the equation E is measured Young's modulus with porosity, E_0 is intrinsic Young's modulus for fully dense material, P is the volume fraction of porosity and b is a shape factor characteristic of the type of porosity:

$$E = E_0 e^{-bP} \quad (7)$$

For porosity in this system, a value of 4 was assumed for b based on the value of 3.92 determined for Al_2O_3 with closed, rounded porosity [33]. Using the measured volume fraction of porosity for the hot pressed material (1.7%), a value of 392 GPa was calculated for E_0 . Using a value of 0.19 (typical for ZrC^{32}) for Poisson's ratio, G_0 was then calculated to be 165 GPa. The E_0 and G_0 values are plotted as open circles at zero volume fraction of Mo in Fig. 4. These values were then used as input for the models used to compare to the elastic moduli of the ZrC–Mo composites.

Several models have been developed to predict the elastic moduli of multi-phase materials [34,35]. The Hashin and Shtrikman relation [34] uses the shear and bulk moduli of the material, along with volumetric and stored energy considerations for each phase, to define the upper and lower bounds on the moduli with respect to the volume fraction of a second phase. Another model proposed by Fan et al. [35] combines a volumetric rule of mixtures with the phase contiguity proposed by Gurland [27]. The combination predicted

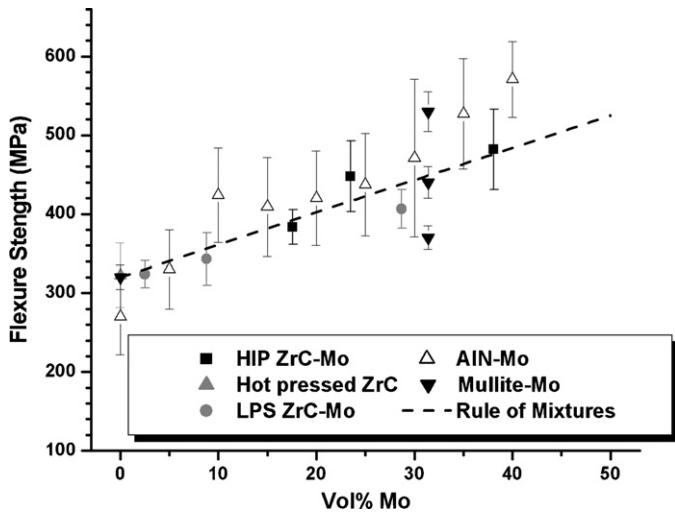


Fig. 5. Flexure strength as a function of Mo content for materials in this study as well as other ceramic Mo composites.

elastic modulus values that fell between the Hashin and Shtrikman bounds for several different systems [35]. Both of these methods were applied in the present study, and it was determined that the predictions were essentially indistinguishable (within 1 GPa) from one another and from a normal volumetric rule of mixtures over the range of compositions studied. These models are represented by the “calculated” values in Fig. 4 and were all consistent with the experimental values measured in this study.

3.5. Flexure strength

The strength of the HIP materials increased with increasing Mo content (Fig. 5), as was the case with the liquid phase sintered (LPS) ZrC–Mo composites [15] (also included in Fig. 5). The lowest strength was exhibited by the hot pressed ZrC (320 MPa) and the highest with the 40 vol% Mo HIP material (480 MPa).

Previous studies have observed the effect of Mo additions on the strength of AlN [18,19] and mullite [36]. The flexure strength results of these studies are also included in Fig. 5. The strengths of both the baseline AlN (270 MPa) mullite (320 MPa) were similar to the baseline ZrC in this study. As with the ZrC in this study, the addition of Mo to AlN and mullite increased the strengths of these other cermet. Taking the experimental error into account for the HIP and LPS ZrC–Mo composites, the strengths of all of the materials were nearly identical as Mo content increased.

Fig. 5 also includes a simple volumetric rule of mixture analysis of strength assuming the measured of 320 MPa strength for ZrC, and a yield strength of 730 MPa, which has been reported for a TZM alloy [31,37]. This rule of mixtures makes physical sense when considering the theory presented by Gurland on the strength of two-phase materials [28]. In Gurland’s study, the strength of a two-phase material was taken to be a volumetric rule of mixtures with a contiguity term (Eq. (8)), where σ is strength, C is contiguity, and f is volume fraction with the subscripts C, M, H denoting composite, metal, and hard phases, respectively:

$$\sigma_C = \sigma_M(1 - C_H f_H) + \sigma_H C_H f_H \quad (8)$$

The physical basis for this model is that a “skeleton” is formed by the hard phase that supports the load and is reinforced with the metal phase, which describes the strength and hardness behavior of WC–Co cermets. It was also determined that WC–Co materials fracture by a process of cracking of the carbide, followed by fracture of the metal ligaments between the carbide grains [38]. This pro-

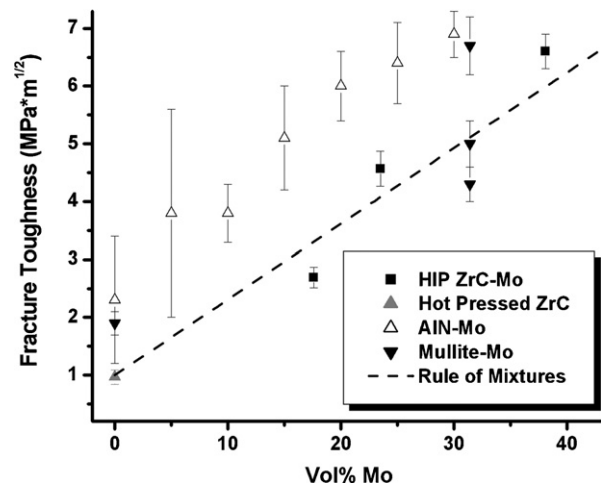


Fig. 6. Fracture toughness (K_{IC}) values for the materials tested in this study as well as for other ceramic–Mo composites.

cess is aided by the large difference in Young’s modulus between WC and Co (700 GPa for WC compared to 210 GPa for Co) [35]. In the ZrC–Mo composites considered in this study, the difference in elastic moduli is much less, with the ZrC being only ~60 GPa higher than the Mo. In the case of the AlN–Mo and mullite–Mo composites, the ceramic phases actually have lower Young’s moduli than Mo. In these materials, the Mo is able to behave as part of the “skeleton.” For the cases where the moduli of the ceramic are equal to or less than the modulus of the Mo, the contiguity term (C) in Eq. (8) essentially goes to unity, and all that is left is a volumetric rule of mixtures.

3.6. Fracture toughness

The flexure strength results are complemented by the fracture toughness results and aid in more fully understanding the fracture behavior of the ZrC–Mo composites (Fig. 6). Fracture toughness increased with increasing Mo content. Hot pressed ZrC had the lowest fracture toughness (1.0 MPa \sqrt{m}) and the 40 vol% Mo composition had the highest toughness (6.6 MPa \sqrt{m}). The value for ZrC is significantly less than the previously reported literature value [3]. The low fracture toughness of the ZrC baseline material could be due to the difference in the methods used to measure fracture toughness. The method used in the previous study used a single edge notched beam (SENB), but did not specify a method for creating a sharp crack. Failure to create a sharp crack would cause an increase in the measured fracture toughness [39]. The general increase in fracture toughness with increasing Mo content was also observed in the AlN–Mo [18,19] and mullite–Mo [36] composites (Fig. 6). The AlN–Mo materials had higher fracture toughness values for all Mo values than the ZrC–Mo materials in the present study, but the values appear to increase with increasing Mo content at approximately the same rate. The toughness of the sintered mullite–Mo materials (the two lower values at 31 vol% Mo) appeared to be consistent with the toughness of the HIP ZrC–Mo for the same amount of Mo in the pressurelessly sintered materials, but the toughness increased to about the same value as the hot pressed AlN–Mo when the mullite–Mo material was hot pressed (highest mullite–Mo value at 31 vol% Mo).

A volumetric rule of mixtures is also plotted in Fig. 6, assuming a measured fracture toughness of 1.0 MPa \sqrt{m} for pure ZrC and a toughness of 14.1 MPa \sqrt{m} for the Mo phase [37]. The rule of mixtures calculation appears to predict the general trend in the fracture toughness values for the HIP ZrC–Mo materials. Despite having

Table 3

The critical flaw size of hot pressed ZrC and HIP ZrC–Mo materials as determined by the Griffith fracture criterion

Material	Strength (MPa)	K_{IC} (MPa \sqrt{m})	Critical flaw size (μm)
Hot pressed ZrC	323	1.0	3
HIP ZrC–20% Mo	383	1.0	16
HIP ZrC–30% Mo	448	2.7	33
HIP ZrC–40% Mo	482	4.6	60

higher values, the toughness values for AlN–Mo also seem to exhibit a trend that can be described as linear. This corroborates the flexure strength results, in that the crack resistance of the material is proportional to the volume of Mo that a crack must propagate through in order to fracture the material.

Using the Griffith criterion (Eq. (9)) [40] along with the measured fracture toughness (K_{IC}) and strength values (σ_f), the critical flaw size (c) was calculated for the ZrC–Mo composites (Table 3):

$$c = \frac{K_{IC}^2}{\pi\sigma_f^2} \quad (9)$$

The results of the critical flaw size analysis add some additional insight to the flexure strength results. For hot pressed ZrC, the predicted critical flaw size was $\sim 3 \mu\text{m}$, which is well below the size of the largest grain that was observed ($\sim 50 \mu\text{m}$). The calculated critical flaw size was also less than the average grain size ($\sim 10 \mu\text{m}$) measured for the hot pressed material. Instead, this critical flaw size appears to correspond more closely with the size of the pores observed in the microstructure, which had an average size of $\sim 1.5 \mu\text{m}$ and a maximum size of $\sim 3.5 \mu\text{m}$.

The HIP materials exhibited an appreciable increase in the critical flaw size (16–60 μm) as compared to the pure ZrC. Considering the microstructures of the materials (Fig. 2) and the Mo cluster sizes determined by image analysis, the critical flaw size in the HIP materials seemed to correspond with the observed size of the Mo clusters. This is consistent with fracture surface examination from the flexure testing, where the fractures appeared to originate in clusters of Mo at or near the tensile surface of the specimens. Thus, it can be concluded that the Mo clusters are the critical flaws in the HIP ZrC–Mo materials.

4. Summary

ZrC–Mo composites with nominally 20, 30 and 40 vol% Mo were produced using HIP. All of the compositions reached near full density after HIP processing at 1800 °C and 200 MPa for 1 h. For comparison, pure ZrC hot pressed at 2200 °C and 30 MPa for 1 h achieved $\sim 98\%$ of its theoretical density.

XRD analysis of the ZrC–Mo composites showed that the 20 and 40 vol% Mo compositions consisted of only (Zr,Mo)C and Mo solid solution, while the 30 vol% also contained a small amount of (Mo,Zr)₂C. Using Rietveld analysis, the amount of Mo contained in the ZrC structure was found to increase with nominal Mo content from $\sim 6 \text{ mol}\%$ for the 20% Mo material to $\sim 8 \text{ mol}\%$ for the 40% Mo material. The actual Mo contents (nominal composition less the amount going into solid solution in ZrC) of the materials were then used for the mechanical properties analyses.

Hardness decreased with increasing Mo content with hot pressed ZrC having a hardness of $\sim 20 \text{ GPa}$, and decreasing to $\sim 8 \text{ GPa}$ for the nominally 40 vol% Mo material. The decrease in hardness was consistent with the Enqvist et al. relation, once the baseline hardness of ZrC was adjusted to account for the presence of a small volume fraction of porosity in the material. This suggested that the hardening effect of constraining the Mo phase in the material governs the overall hardness of the composite.

Hot pressed ZrC had the lowest Young's and shear moduli of all the materials in the study. Once the elastic moduli of ZrC were adjusted to compensate for the presence of porosity, the trends in the elastic moduli were consistent with several rules of mixtures relations, even a simple volumetric rule of mixtures. The predicted elastic moduli were all essentially identical due to the similarity values of Young's moduli for the ZrC phase and the Mo phase (392 GPa versus 330 GPa).

The flexure strength of the ZrC–Mo composites increased with increasing Mo content to a maximum of $\sim 480 \text{ MPa}$ at 40 vol% Mo. The increase in strength with increasing Mo additions was consistent with AlN–Mo and mullite–Mo composites from the technical literature. All of the Mo composites increased in strength with increasing Mo content that can generally be described by a linear rule of mixtures. The rule of mixtures trend can be explained physically by the similarity of elastic moduli between the ceramic and Mo phases. This leads to load support in fracture testing determined by the volume fraction of each phase.

Fracture toughness increased linearly with Mo content, from 1.0 MPa \sqrt{m} for hot pressed ZrC to 6.6 MPa \sqrt{m} for ZrC with 40 vol% Mo. The increase in fracture toughness was also consistent with the increases in fracture toughness observed for some AlN–Mo and mullite–Mo composites. The increasing fracture toughness can be generally described with the rule of mixtures calculation similar to the strength measurements. The fracture toughness values also suggest that the critical flaws in the HIP ZrC–Mo composites are the clusters of Mo observed in the microstructures.

References

- [1] E. Rudy, Compendium of Phase Diagram Data, Air Force Materials Laboratory Metals and Ceramics Division, Wright-Patterson AFB, OH, 1969, p. 162.
- [2] E.E. Kotlyar, T.N. Nazarchuk, Chemical properties of carbides of transition metals of groups IV and V, *Inorg. Mater.* 2 (1966) 1532–1538.
- [3] E. Min-Haga, W.D. Scott, Sintering and mechanical properties of ZrC–ZrO₂ composites, *J. Mater. Sci.* 23 (1998) 2865–2870.
- [4] W.G. Lidman, H.J. Hamjian, Reactions during sintering of a zirconium carbide–niobium cermet, *J. Am. Ceram. Soc.* 35 (1952) 236–240.
- [5] G.M. Song, Y. Zhou, Y.J. Wang, T.C. Lei, Elevated temperature strength of a 20 vol% ZrC_p/W composite, *J. Mater. Sci. Lett.* 17 (1998) 1739–1741.
- [6] G.M. Song, Y.J. Wang, Y. Zhou, Elevated temperature ablation resistance and thermophysical properties of tungsten matrix composites reinforced with ZrC particles, *J. Mater. Sci.* 36 (2001) 4625–4631.
- [7] M.B. Dickerson, P.J. Wurm, J.R. Schorr, W.P. Hoffman, P.G. Wapner, K.H. Sandhage, Near net-shape, ultra-high melting, recession-resistant ZrC/W-based rocket nozzle liners via the displacive compensation of porosity (DCP) method, *J. Mater. Sci.* 39 (2004) 6005–6015.
- [8] T. Suzuki, H. Matsumoto, N. Nomura, S. Hanada, Microstructures and fracture toughness of directionally solidified Mo–ZrC eutectic composites, *Sci. Tech. Adv. Mater.* 3 (2002) 137–143.
- [9] T. Suzuki, H. Matsumoto, N. Nomura, S. Hanada, Microstructures and mechanical properties of eutectic Mo–XC (X = Ti, Zr, Hf) in situ composites, *Trans. Mater. Res. Soc. Jpn.* 26 (2001) 307–310.
- [10] T. Suzuki, H. Matsumoto, N. Nomura, S. Hanada, Microstructure and creep of Mo–ZrC in situ composite, *Mater. Trans.* 41 (2000) 1164–1167.
- [11] T.C. Wallace, C.P. Gutierrez, P.L. Stone, The molybdenum–zirconium–carbon system, *J. Phys. Chem.* 67 (1963) 76–801.
- [12] T.F. Fedorov, Yu.B. Kuz'ma, L.V. Gorshkova, Phase equilibria in the ternary system zirconium–molybdenum–carbon, *Sov. Powder Metall. Met. Ceram.* 3 (1965) 229–233.
- [13] H. Holleck (Ed.), Binäre und ternäre Carbide und Nitride der Übergangsmetalle und ihre Phasenbeziehungen, Kernforschungszentrum Karlsruhe, Karlsruhe, Germany, 1981, pp. 161–162.
- [14] S.E. Landwehr, G.E. Hilmas, W.G. Fahrenholtz, I.G. Talmy, Processing of ZrC–Mo cermets for high-temperature applications. Part I. Chemical interactions in the ZrC–Mo system, *J. Am. Ceram. Soc.* 90 (7) (2007) 1998–2002.
- [15] S.E. Landwehr, G.E. Hilmas, W.G. Fahrenholtz, I.G. Talmy, "Processing of ZrC–Mo Cermets for High Temperature Applications, Part II: Pressureless Sintering and Mechanical Properties", *J. Am. Ceram. Soc.* 91 (3) (2008) 873–878.
- [16] M.N. Rahaman, Ceramic Processing, Taylor & Francis, Boca Raton, 2007.
- [17] Metals and Ceramics Information Center, Hot Isostatic Processing, Battelle Columbus Laboratories, Columbus, OH, 1982.
- [18] A.A. Khan, J.C. Labbe, Aluminum nitride–molybdenum ceramic matrix composites: influence of molybdenum addition on mechanical properties, in:

- Proceedings of the 5th International Symposium in Advanced Materials, 1997, pp. 49–56.
- [19] A.A. Khan, J.C. Labbe, Aluminium nitride–molybdenum ceramic matrix composites. Influence of molybdenum addition on electrical, mechanical and thermal properties, *J. Eur. Ceram. Soc.* 17 (1997) 1885–1890.
- [20] R.E. Taylor, Thermal conductivity of zirconium carbide at high temperatures, *J. Am. Ceram. Soc.* 45 (7) (1962) 353–354.
- [21] J.Z. Briggs, Properties and Selection: Nonferrous Alloys and Special-Purpose Materials, in: S.R. Lampman (Ed.), *ASM Metals Handbook*, vol.2, ASM International, 1990, pp. 1140–1143.
- [22] P. Barnier, C. Brodhag, F. Thevenot, Hot-pressing kinetics of zirconium carbide, *J. Mater. Sci.* 21 (7) (1986) 2452–2547.
- [23] A.G. Lanin, E.V. Marchev, S.A. Pritchin, Non-isothermal sintering parameters and their influence on the structure and properties of zirconium carbide, *Ceram. Int.* 17 (5) (1991) 301–307.
- [24] G.V. Samsonov, R.Ya. Petrikina, Sintering of metals, carbides, and oxides by hot-pressing, *Phys. Sint.* 2 (3) (1970) 1–20.
- [25] H. Lee, J. Gurland, Hardness and deformation of cemented tungsten carbide, *Mater. Sci. Eng.* 33 (1978) 125–133.
- [26] H.A. Calderon, G. Kostorz, G. Ullrich, Microstructure and plasticity of two molybdenum-base alloys (TZM), *Mater. Sci. Eng. A* A160 (1993) 189–199.
- [27] J. Gurland, The measurement of grain contiguity in a two phase material, *Trans. Met. Soc. AIME* 212 (1958) 452–455.
- [28] J. Gurland, A structural approach to the yield strength of two-phase alloys with coarse microstructures, *Mater. Sci. Eng.* 40 (1979) 59–71.
- [29] H. Enqvist, S. Jacobson, N. Axén, A model for the hardness of cemented carbides, *Wear* 252 (2002) 384–393.
- [30] C.M. Wu, R.W. Rice, Porosity dependence of wear and other mechanical properties on fine-grain Al_2O_3 and B_4C , *Ceram. Eng. Sci. Proc.* 6 (7–8) (1985) 977–994.
- [31] G. Filacchioni, E. Casagrande, U. De Angelis, G. De Santis, D. Ferrara, Effects of strain rate on tensile properties of TZM and Mo–5%Re, *J. Nucl. Mater.* 307–311 (2002) 705–709.
- [32] Battelle Metals and Ceramics Information Center, *Engineering Data on Selected Ceramics*, vol. II. Carbides, Battelle Columbus Laboratories, Columbus, OH, 1979.
- [33] R.M. Spriggs, Expression for effect of porosity on elastic modulus on polycrystalline refractory materials, particularly aluminum oxide, *J. Am. Ceram. Soc.* 45 (1961) 94.
- [34] Z. Hashin, S. Shtrikman, A variational approach to the theory of the elastic behavior of polycrystals, *J. Mech. Phys. Sol.* 10 (1962) 343–352.
- [35] Z. Fan, P. Tsakirooulos, A.P. Miodownik, Prediction of Young's modulus of two phase composites, *Mater. Sci. Technol.* 8 (1992) 922–929.
- [36] J.F. Bartolomea, M. Diaz, J. Requena, J.S. Moya, A.P. Tomsia, Mullite/molybdenum ceramic–metal composites, *Acta Mater.* 47 (14) (1999) 3891–3899.
- [37] B.V. Cockeram, The mechanical properties and fracture mechanisms of wrought low carbon arc cast (LCAC), molybdenum–0.5pct titanium–0.1pct zirconium (TZM), and oxide dispersion strengthened (ODS) molybdenum flat products, *Mater. Sci. Eng. A* 418 (2006) 120–136.
- [38] L.S. Sigl, H.E. Exner, Experimental study of the mechanics of fracture in WC–Co alloys, *Met. Trans. A* 18A (1987) 1299–1308.
- [39] A. Ghosh, M.G. Jenkins, K.W. White, A.S. Kobayashi, R.C. Brad, Elevated-temperature fracture resistance of a sintered α -silicon carbide, *J. Am. Ceram. Soc.* 72 (2) (1989) 242–247.
- [40] J.B. Wachtman, *Mechanical Properties of Ceramics*, John Wiley & Sons, New York, 1996.